

Simplifying Multimodality: Unimodal Approach to Multimodal Challenges in Radiology with General-Domain Large Language Model

Seonhee Cho

*Kim Jaechul Graduate School of AI
KAIST
Seongnam, Gyeonggi, Korea*

SEONHEE.CHO@KAIST.AC.KR

Choonghan Kim

*Moon Soul Graduate School of Future Strategy
KAIST
Daejeon, Korea*

CHOONGHANKIM@KAIST.AC.KR

Jiho Lee

*Department of Computer Science and Engineering
Ewha Womans University
Seoul, Korea*

Chetan Chilkunda

*Department of Chemical Engineering
Carnegie Mellon University
Pittsburgh, PA, USA*

Sujin Choi

*Division of Environmental Science and Engineering
POSTECH
Pohang, Gyeongbuk, Korea*

Joo Heung Yoon*

*Division of Pulmonary, Allergy, Critical Care, and Sleep Medicine
Department of Medicine
University of Pittsburgh
Pittsburgh, PA, USA*

YOONJH@UPMC.EDU

Abstract

Recent advancements in Large Multimodal Models (LMMs) have attracted interest in their generalization capability with only a few samples in the prompt. This progress is particularly relevant to the medical domain, where the quality and sensitivity of data pose unique challenges for model training and application. However, the dependency on high-quality data for effective in-context learning raises questions about the feasibility of these models when encountering with the inevitable variations and errors inherent in real-world medical data. In this paper, we introduce MID-M, a novel framework that leverages the in-context learning capabilities of a general-domain Large Language Model (LLM) to process multimodal data via image descriptions. MID-M achieves a comparable or superior performance

* Corresponding author

to task-specific fine-tuned LMMs and other general-domain ones, without the extensive domain-specific training or pre-training on multimodal data, with significantly fewer parameters. This highlights the potential of leveraging general-domain LLMs for domain-specific tasks and offers a sustainable and cost-effective alternative to traditional LMM developments. Moreover, the robustness of MID-M against data quality issues demonstrates its practical utility in real-world medical domain applications.

1. Introduction

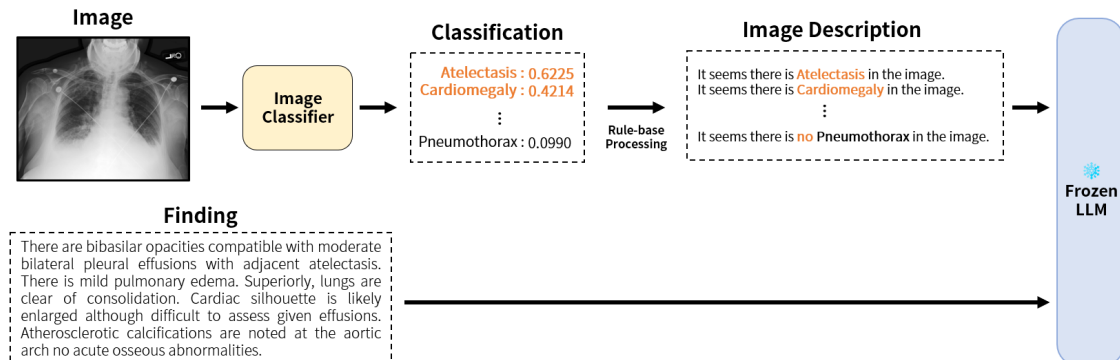
Recently, large multimodal models (LMMs) have made significant progress, becoming capable of interpreting and integrating information across different data types, such as text and images (Achiam et al., 2023; Driess et al., 2023). This progress closely aligns to advancements in Large Language Models (LLMs), since many LMMs are built upon the structural foundation of pre-trained LLMs (Touvron et al., 2023; Chiang et al., 2023). Consequently, attempts to use LMM’s in-context learning capability without fine-tuning on specific tasks are increasing (Wei et al., 2022; Zhang et al., 2023b). This tendency also appears in the medical domain, where the data collection is challenging due to the concerns on using sensitive clinical information containing re-identifiable patient data (Benitez and Malin, 2010) and the expensive labeling process which requires expert knowledge.

However, the performance of in-context learning approach is highly susceptible to the data quality (Liu et al., 2023). One primary cause of degrading data quality is data loss occurring during the data collection and curation process, even when guided by expert input. For instance, the analysis of radiographic images has reported an error rate of 3 to 5% (Robinson et al., 1999) and the problem appears challenging to resolve until now (Brady, 2017). Similarly, a basic chart review showed electronic health record (EHR) errors could reach 9 to 10% (Feng et al., 2020). Additionally, variations in data interpretation by medical professionals are quite common (Whiting et al., 2015) and this can further exacerbate these issues by adding another layer of complexity to ensuring the quality and consistency of data.

In this paper, we introduce **MID-M**, a **M**ultimodal framework with **I**mage **D**escription for **M**edical domain. It is an in-context learning framework that demonstrates robust performance even with low-quality data. Our framework uses general-domain LLM and leverages multimodal data by converting images to textual descriptions. Notably, it achieves comparable performance to other general-domain and fine-tuned LMMs without pre-training on multimodality and extensive fine-tuning for the medical domain. In addition, by processing the image as a text description, it has the advantage of representing the image in an accessible and interpretable way, compared to traditional embedded vector representations. Our framework is illustrated in Figure 1.

To evaluate the model’s performance in the scenario with low-quality data, we systematically mask the texts in a medical dataset and make the new adversarial evaluation data. We compare the performance of general domain pre-trained and medically fine-tuned LMM models to our framework in a few-shot setting, focusing on their accuracy and semantic comprehensibility. Through this experiment, we aim to assess the effectiveness of LMMs in generalizing to domain-specific tasks and managing incomplete source data.

Figure 1: Overview of MID-M framework.



Generalizable Insights about Machine Learning in the Context of Healthcare

In this study, we analyze the generalization capabilities of LLMs and LMMs across various dimensions. First, we investigate the ability of models trained in general domains to effectively generalize to medical texts through few-shot learning. This aligns with the recent trend towards adopting eco-friendly approaches in AI model training by reducing the need for massive pretraining and extensive fine-tuning. It also contributes to the validation of model’s potential to generalize well across any domain or task, as aimed for in general domain research. Second, we verify the models’ ability to generalize in situations where data quality deteriorates. The challenge that in-context learning models are easily influenced by the number of few-shot samples and the quality of trained data remains unresolved. Therefore, concrete evaluation in this regard is crucial for the advancement of models.

Furthermore, our research reveals that text-only models can efficiently handle multimodal healthcare tasks with less computational demand. We demonstrate that smaller language models can achieve results comparable to larger models, indicating a path for wider adoption of AI in healthcare, especially in resource-limited settings in computation or a lower level of healthcare environment. This goes in line with a move towards developing globally accessible AI solutions by the National Institutes of Health¹, highlighting the potential utility of proposed research in expanding AI’s reach.

2. Background

In this section, we review the relevant literature on large language or multimodal models in the general domain as well as those applied specifically to the tasks in healthcare.

2.1. Large Language Models for Vision and Language Tasks

Multimodal pretraining Large multimodal models have often leveraged language models as the backbone architecture and incorporate methods to connect the image encoder with the language model (Awadalla et al., 2023; Alayrac et al., 2022; Li et al., 2023a,b; Xu et al., 2024; Laurençon et al., 2024; Liu et al., 2024; Dai et al., 2024). Notably, LLaVA (Liu

1. <https://commonfund.nih.gov/bridge2ai>

et al., 2024) employs a direct projection layer, BLIP-2 (Li et al., 2023b) uses a lightweight Q-Former, and Flamingo (Alayrac et al., 2022) uses gated cross-attention, to name a few examples.

However, this paradigm suffers from two critical drawbacks. First, pretraining requires a high computational burden. Jointly aligning vision backbones and large language models requires large computational resources, despite considerably fewer trainable parameters compared to the total parameters. For example, Flamingo takes two weeks with 1,536 TPUs for the largest run, and BLIP-2 takes around 10 days with 16 A100 GPUs. Hence, it becomes prohibitively expensive to switch to a different large language model. The second limitation is the lack of modularity and flexibility. Even though they integrate pretrained image encoder and frozen LLM, updating this integrated system demands training the network with substantial data instances and time (Laurençon et al., 2024), hindering iterative research and development.

Multimodal Reasoning with Language There have also been approaches that attempt to tackle multimodal tasks using language models alone (Yang et al., 2022; Guo et al., 2022; Hu et al., 2022; Xie et al., 2022; Surís et al., 2023; Berrios et al., 2023). Among these, LENS (Berrios et al., 2023) is particularly relevant to our work, as this framework extracts generic information such as tags, attributes, and captions with three different vision modules, and provides them to the language model. While this method can be beneficial for general domain tasks, such an approach does not scale well to tasks that require expert knowledge. In contrast, our framework facilitates LLM’s multimodal reasoning within the medical domain. We introduce a more streamlined framework with a single ‘vision module’ and tailor a general domain LLM specifically for medical tasks, by leveraging the adaptability of the LLM in this knowledge-intensive domain.

2.2. Large Language Models for Healthcare Domain

Several efforts have been made to specialize these general-purpose foundation models through fine-tuning on healthcare domain-specific data (Li et al., 2024; Moor et al., 2023; Zhang et al., 2023a; Wu et al.; Tu et al., 2024; Sun et al., 2023). However, task-specific fine-tuning is often inefficient, requiring large amounts of high-quality medical data and extensive computing resources.

Consequently, efficient adaptation methods are also explored, which primarily follow two categories: lightweight fine-tuning techniques (Hu et al., 2021; Houlsby et al., 2019), and leveraging the models’ in-context learning capabilities in a few-shot setting. While fine-tuned models generally outperform their counterparts in few-shot setting (Van Veen et al., 2023b,a; Lewis et al., 2020), there is a growing interest in exploring domain adaptation techniques, mainly in-context learning, which do not require additional training (Agrawal et al., 2022; Liévin et al., 2023; Byra et al., 2023; Yan et al., 2023; Nori et al., 2023; Van Veen et al., 2023a). In-context learning has many potential advantages for the clinical domain because there is often a limited set of labeled data due to the high level of expertise needed for annotation. Our work also aligns with this in-context learning approach. By leveraging the capabilities of general-purpose LLMs without additional fine-tuning, our approach aims to overcome the limitations of task-specific fine-tuning while maintaining the models’ broad knowledge and generalization abilities.

3. Methods

This section introduces **MID-M**, an efficient in-context learning framework that performs multimodal tasks using only small-sized language models. MID-M consists of two key components: a domain-specific image converter and a general-domain language model.

Image Conversion with Domain-Specific Image Classifier To reformulate vision-language tasks to text-to-text task, we first extract key information from images and convert it to text. Taking inspiration from *Classification-via-Description* (Menon and Vondrick, 2022) which showed good generalization performance, we employ a *Description-via-Classification* strategy. *Classification-via-description* involves generating textual features representing each class with a language model, then analyzing whether the input exhibits those features to make the final classification decision. Conversely, we use the classification result to generate an image description. Note that using a general-domain image module trained only on generic data, as in Berrios et al. (2023), cannot yield meaningful classification results since chest X-rays require domain knowledge. Therefore, we utilize a SOTA model (Chong et al., 2023) for CheXpert, a publicly available large chest X-ray classification dataset. This classifier computes a probability of 14 major diseases for chest radiology images. For diseases that the classifier predicts to have a probability of presence greater than 20%, we use the sentence “It seems there is $\{disease\}$ in the image.” Conversely, for diseases predicted as absent, we use “It seems there is no $\{disease\}$ in the image.” These sentences describing the presence or absence of each disease are all concatenated and used as an image description. This method can be extended to other domains without domain expertise, by simply replacing the classifier with a domain-specific one. We provide an example of our prompt in Appendix A.

General-domain LLM We utilize a general-domain language model for multimodal reasoning. While chains-of-thought (Wei et al., 2022) are generally advantageous for domain adaptation and complex reasoning, their benefits are not consistent across generation tasks (Kim et al., 2023). Furthermore, it requires domain knowledge to generate rationales. Thus, we utilize strategies known to be helpful for domain adaptation (Van Veen et al., 2023a) instead. Specifically, we prepend a sentence assigning the role of an AI assistant as a domain expert: “You are an expert medical professional.” This is followed by a detailed task description crafted for the radiology domain. For the few-shot examples, we provide the image description, corresponding finding, and impression in sequence. During inference, we omit the impression from the examples to be completed by the model. We use a BM25 retriever, known for its capability to compute token overlap quickly and retrieve relevant examples effectively.

4. Dataset

We utilized the MIMIC-CXR dataset (Johnson et al., 2019), a de-identified and publicly available chest radiograph database collected from 2011 to 2016. It has a total number of 227,835 images and 128,032 paired reports from 65,379 patients. Paired reports include *finding* and *impression*. A *finding* is a detailed observation made from the X-ray images written by radiologists, and an *impression* is a concise summary of the *finding* which becomes the primary mode of communication between medical professionals.

Table 1: Example of MIMIC-CXR findings with different masking rate.

Full	Corrupted 0.1	Corrupted 0.3	Corrupted 0.5
PA and lateral views of the chest provided. AICD projects over the left chest wall with lead tip extending to the region of the right ventricle. The heart is mildly enlarged. There is no evidence of pneumonia or CHF. No effusion or pneumothorax seen. Bony structures are intact.	PA and lateral views of the chest provided. AICD projects over the chest wall with lead tip extending to the region of the right ventric.. heart is mildly enlarged. there is no of pneumonia or CHF. effusion or pneumothorax seen. Bony structures are intact.	PA and lateral of chest provided. CD projects over the left wall with lead tip to the region of the ventric the heart is of pneumonia or CH. no effusion or pneum.rax seen. intact.	PA and lateral views of provided. AI the chest with tip to the vent heart is enlarged. there no F no usion or pneum.rax structures are intact

Preliminary Analysis Our examination of the MIMIC-CXR dataset revealed 3,146 samples (2.46% of the total) that were unsuitable for research due to one or more of the following reasons: the *finding* label contained fewer than three words, was shorter than the *impression* label, or had more than three words masked. This level of incompleteness aligns with error rates reported in previous studies (Robinson et al., 1999).

Pre-preprocessing To prepare the data for our study, we first merged the original training, validation, and test sets. We then removed samples with the *findings* at both extremes of length, removing the shortest and longest 25% of findings to ensure a meaningful level of detail remained after applying masking techniques. This process resulted in a dataset of 64,613 images and reports, which we then randomly split into training, validation, and test sets containing 62,613, 1,000, and 1,000 samples, respectively.

Masking To further evaluate the robustness of LLMs against incomplete data, we employed a masking technique akin to that used by BERT (Devlin et al., 2018), randomly deleting words or phrases at subword levels. We conducted masking at three different rates to the original test set and yielded four distinct test sets: original (*full*), corrupted at 10% (*corrupted 0.1*), corrupted at 30% (*corrupted 0.3*), and corrupted at 50% (*corrupted 0.5*).

We evaluated the effectiveness of our corruption strategy using the F1CheXbert (Zhang et al., 2020) metric. CheXbert (Smit et al., 2020) is designed to identify 14 medical observations in chest X-ray images. The F1CheXbert score is calculated by comparing CheXbert’s predictions on the generated text against the corresponding reference text. We compare the findings from *full* against the findings from each corrupted test set. We discovered a strong correlation between the extent of text corruption and the precision of disease mentions. The micro-average F1CheXbert scores were 91.2% for the 10% corrupted set, 69.3% for the 30% corrupted set, and 51.1% for the 50% corrupted set. Examples of corrupted text are illustrated in Table 1.

5. Experimental Setup

5.1. Task

In this study, the task requires the model to generate an impression based on an X-ray image and its corresponding findings. For all experiments, we employed a 2-shot learning approach, utilizing the BM25 algorithm to retrieve two training samples with findings similar to the findings of the test sample. When experimenting with corrupted test sets, the samples are retrieved based on the corrupted findings. This task is designed to comprehensively evaluate the model’s ability to understand medical images and clinical data, as well as to identify salient information even when incomplete data is given.

5.2. Baselines

We have two groups of baselines in our experiments: LMMs that are pre-trained in the general domain and those further fine-tuned with medical domain data. However, considering the constraints of a few-shot learning setting, we found a limited number of LMMs are capable of processing multiple independent images in a single prompt. Notably, Flamingo (Alayrac et al., 2022), is trained on interleaved text and image pairs and supports multiple images. We used its open-sourced version, OpenFlamingo (Awadalla et al., 2023). This functionality is also applied to the models that are based on Flamingo, IDEFICS (Laurençon et al., 2024) and OTTER (Li et al., 2023a). For models trained on data from the medical domain, we selected MedFlamingo (Moor et al., 2023) and RadFM (Wu et al., 2023). MedFlamingo is trained with medical publications and textbooks and is based on OpenFlamingo. RadFM is a specialized model for the radiology domain and pre-trained with large-scale, high-quality multimodal dataset named MedMD. It’s important to note that although MedMD includes MIMIC-CXR, we still chose to include it in our baseline set. Despite data leakage concerns in our *full* test setting, we believe that evaluating the model’s performance on corrupted versions of MIMIC-CXR would provide valuable insights into its robustness and generalization capabilities.

A detailed comparison is presented in Table 2. Note that all the baseline models have 9 billion parameters or more, whereas our backbone model, Flan-T5-xl, has only 3 billion parameters. For the baselines, we adhered to the example code in their public GitHub repositories when available; otherwise, we utilized a consistent prompt with the example code from other baselines.

5.3. Evaluation

The performance of the models are compared using two different LLM evaluation methods, ROUGE-L (Lin, 2004) and F1RadGraph (Delbrouck et al., 2022). ROUGE, the Recall-Oriented Understudy for Gisting Evaluation, is a metric widely used in the text summarization task. This score evaluates the similarity between the generated text and the reference text based on token overlap. Specifically, we used ROUGE-L which measures the longest common subsequence (LCS) to assess similarity at the sentence level. F1RadGraph is a metric that evaluates medical entities and relations within the generated reports. It utilizes a PubMedBERT (Gu et al., 2021) fine-tuned on the RadGraph (Jain et al., 2021), a dataset with chest X-ray radiology reports annotated with medical entities and their relations. This

Table 2: Descriptions of baseline models. The first four models are general-domain LMMs that can handle multiple images in one input. The two models in the middle are LMMs that are fine-tuned with medical domain data.

Model	Size	Domain	Image Encoder	Language Model
Otter _M	9B	General	ViT-L/14	MPT-7b
Otter _L	9B	General	ViT-L/14	LLaMA-7b
OpenFlamingo	9B	General	ViT-L/14	MPT-7b
IDEFICS	9B	General	ViT-H/14	LLaMA-7b
MedFlamingo	9B	Medical	ViT-L/14	LLaMA-7b
RadFM	14B	Radiology	ViT-B/32	MedLLaMA-13b
MID-M	3B	General	Classifier(7M)	Flan-T5-xl

fine-tuned PubMedBERT model identifies the entities and relations from the generated reports and the reference reports. When the generated report correctly matches the entities and their relation to that in the reference, they receive a reward of 1, and otherwise, 0. The final F1 score is computed based on this reward score. Both metrics are implemented using the Python Package Index (PyPI)²

6. Experiment

6.1. Result

The experimental results are presented in Table 3. MID-M achieves performance comparable to that of other baseline models in all settings, despite using only a third of the parameters. It even surpasses other models in experiments with corrupted data, highlighting its exceptional generalization capabilities. RadFM, which previously trained on MIMIC-CXR, achieves the highest score on the *full* test set, which is not a surprising result. IDEFICS and OpenFlamingo demonstrate strong generalization ability, achieving scores around 0.4 across both ROUGE and F1RadGraph metrics.

However, we observed that some models are highly sensitive to even a minor level of data corruption (i.e. 0.1). For instance, RadFM suffers from a significant performance drop in corrupted settings and shows performance similar to or even worse than large-scale general domain models. This sensitivity to text corruption is likely due to its training on only high-quality radiology images and associated texts. It is critical problem in clinical applications where even small decreases in performance can significantly impact patient care. Otter and OpenFlamingo also shows considerable performance declines in corrupted settings. Conversely, IDEFICS, MedFlamingo and our framework maintain robust performance on low-quality data. As the text masking probability increases (i.e. 0.3, 0.5), our model begins to demonstrate its full potential. It achieves the highest scores under the ROUGE metric and exhibits either comparable or superior performance on the F1RadGraph metric.

2. <https://pypi.org/project/radgraph/>

Table 3: Model performances in each test set with regard to the accuracy. The highest score is bolded and the second highest is underlined.

Method	<i>Full</i>	<i>Corrupted 0.1</i>	<i>Corrupted 0.3</i>	<i>Corrupted 0.5</i>
<i>ROUGE</i>				
Otter _M	0.3140	0.2258	0.2116	0.1894
Otter _L	0.2655	0.2089	0.1876	0.1461
OpenFlamingo	<u>0.4310</u>	0.3458	<u>0.3420</u>	<u>0.2888</u>
IDEFICS	0.3951	<u>0.3776</u>	0.3321	0.2807
MedFlamingo	0.3804	0.3622	0.3270	0.2784
RadFM	0.5222	0.3952	0.3299	0.2534
MID-M(ours)	0.4064	0.3719	0.3438	0.2977
<i>F1RadGraph</i>				
Otter _M	0.2801	0.2114	0.1704	0.1327
Otter _L	0.2587	0.1994	0.1720	0.1237
OpenFlamingo	0.4030	0.3427	0.3151	0.2541
IDEFICS	<u>0.4089</u>	<u>0.3688</u>	0.3064	<u>0.2543</u>
MedFlamingo	0.3973	0.3510	0.3046	0.2566
RadFM	0.5054	0.3839	<u>0.3094</u>	0.2363
MID-M(ours)	0.3732	0.3379	0.2973	0.2622

It is also surprising that MedFlamingo, which is further fine-tuned from OpenFlamingo with medical domain text, does not outperform OpenFlamingo. This may be because MedFlamingo is primarily fine-tuned for medical visual question-answering tasks rather than various medical generation tasks. These experimental results shows the importance of task setting during pre-training and fine-tuning.

6.2. Ablation Studies

To comprehend the the effect of each component in our framework to the overall performance, we systematically remove each element - textual input (findings), image input (descriptions), and both. In scenarios where both text and images are excluded, the model must generate impressions based solely on two impressions retrieved based on the similarity of findings. The results of these ablation studies are presented in Table 4.

The results indicate that the multimodal framework exhibits the strongest generalization capability by leveraging all available information. Since the impressions are primarily derived from findings, the text component alone proves to be most effective when the text data encompasses sufficient information. Still, using both image and text information achieves comparable scores and outperforms in the corrupted test sets. When text corruption exceeds a 10% probability, incorporating image descriptions improves the model’s accuracy compared to using only the findings or only the image descriptions in most cases. One interesting point is, at the highest level of text corruption, the corrupted text acts as noise

Table 4: Model performances in different input settings.

Method	<i>Full</i>	<i>Corrupted 0.1</i>	<i>Corrupted 0.3</i>	<i>Corrupted 0.5</i>
<i>ROUGE</i>				
MID-M	<u>0.4064</u>	0.3719	<u>0.3438</u>	0.2977
w/o text	0.3794	0.3563	0.3440	<u>0.2942</u>
w/o image	0.4119	<u>0.3683</u>	0.3218	0.2550
w/o text and image	0.3649	0.3309	0.3129	0.2670
<i>F1RadGraph</i>				
MID-M	<u>0.3732</u>	0.3379	0.2973	0.2622
w/o text	0.3354	0.3185	<u>0.2948</u>	<u>0.2575</u>
w/o image	0.3918	<u>0.3323</u>	0.2784	0.2247
w/o text and image	0.3298	0.2976	0.2783	0.2378

and severely impairs the model’s performance, leading to worse outcomes than when both text and images were excluded. This trend remains consistent across evaluation metrics of token overlap, measured by ROUGE, and semantic coherence, measured by F1RadGraph.

6.3. Disease Identification Ability

In this section, we further analyze the model’s ability to identify the major diseases in X-rays and corresponding findings. The evaluation in Section 6.1 is based on a broad comparison of impressions and predictions at the word and semantic level. Additionally in this section, we use the F1CheXbert to assess whether the model identifies all the key diseases noted in the gold impressions in its predictions as well. We report both the micro-average F1 score and the individual F1 scores for five main diseases, as shown in Table 5.

Table 5: Comparison of MID-M’s performance on the identification of major diseases under different levels of data corruption. Abbreviations: CMG, cardiomegaly; Consol, consolidation; Atelect, atelectasis; PE, pleural effusion.

	CMG	Edema	Consol	Atelect	PE	Micro Avg.
<i>Full</i>	0.4200	0.5714	0.4444	0.4916	0.6335	0.5302
<i>Corrupted 0.1</i>	0.3204	0.4923	0.1538	0.4067	0.5543	0.4379
<i>Corrupted 0.3</i>	0.3010	0.3884	0.1176	0.3972	0.4250	0.3724
<i>Corrupted 0.5</i>	0.2631	0.3606	0.1538	0.2704	0.4467	0.3327
Support	87	148	25	151	138	549

We found that the model’s performance declines with increased data corruption, but the rate of decline varies across diseases. For instance, the model’s ability to identify pleural effusion (PE) remains relatively robust against corruption, even under conditions of high data corruption, compared to other diseases. In contrast, our model experiences a significant drop in consolidation (Consol) even at the lowest level of corruption (0.1). This suggests that the model manages to recognize some diseases in a manner less susceptible

Table 6: Model performances in different number of shots in the input prompt.

Method	<i>Full</i>	<i>Corrupted 0.1</i>	<i>Corrupted 0.3</i>	<i>Corrupted 0.5</i>
<i>ROUGE</i>				
0-shot	0.1673	0.1270	0.1127	0.1091
1-shot	0.3818	0.3438	0.3172	0.2180
Ours (2-shot)	0.4064	0.3719	0.3438	0.2977
<i>F1RadGraph</i>				
0-shot	0.1573	0.0994	0.072	0.0439
1-shot	0.3536	0.3091	0.2797	0.2386
Ours (2-shot)	0.3732	0.3379	0.2973	0.2622

to corruption. This might be attributed to the feasibility of retrieving similar samples. When there are many samples with a certain disease in the training set, it becomes easier to retrieve relevant samples for the diseases and vice versa. In addition, a significant drop in consolidation might be attributed to a unique linguistic challenge. When some of the subwords from consolidation are obscured, the remaining segments (such as 'solid' or 'tion') could be mistakenly associated with other terms frequently used in radiology reports, complicating its identification.

6.4. In-Context Learning Ability

In this section, we evaluate the model’s in-context learning capabilities by varying the number of examples (shots) included in the prompt. Previous experiments, as discussed in Section 6.1, uniformly used a two-shot setting. In addition to this, we explore the model’s abilities in zero-shot and one-shot settings. The results are presented in Table 6.

We observe a decline in performance in both zero-shot and one-shot settings compared to the two-shot scenario. However, the disparity in performance across these settings is noteworthy. In the zero-shot setting, the model struggles significantly, achieving a ROUGE score of only about 0.1673 on the full test set and with the F1RadGraph score approaching zero across all corrupted test sets. In contrast, introducing just one relevant example enhances the model’s performance substantially, achieving results that are comparatively close to those in the two-shot setting in many cases. This underscores the impressive in-context learning capabilities of pretrained large models, highlighting their potential for easy adaptation to different domains without the need for fine-tuning.

7. Discussion

In this paper, we introduce MID-M, a novel multimodal framework designed for the medical domain, which leverages the in-context learning capabilities of a general-domain LLM. By transforming images into textual descriptions, MID-M facilitates an interpretable representation of medical images, enabling complex information to be more accessible to engineers and, potentially, to practitioners. Notably, MID-M demonstrates superior generalization capability, outperforming models with substantially more parameters that are extensively

trained for multimodality and medical applications. This emphasizes the potential of leveraging general-domain models for specialized tasks, offering a sustainable and cost-effective approach without massive pretraining and extensive fine-tuning. This approach aligns with the ongoing shift towards developing powerful AI tools in healthcare. Furthermore, it highlights the importance of robustness and generalization in systems, particularly in healthcare settings where data quality can vary significantly. The framework’s ability to maintain robust performance even with degraded data quality, presents a compelling case for its application in real-world medical scenarios even with limited resources. We hope our work can contribute to the development of globally accessible AI systems.

Limitations Despite the contributions of our research, there are a few limitations to our work. First, while MID-M demonstrates superior in-context learning capability, it still underperforms compared to task-specific fine-tuned models. This is observed from the performance of RadFM on the *full* test set. However, it is important to note that models like RadFM demand high computational resources for their training and show a significant drop in generalization ability when faced with incomplete data. In future works, we could focus on developing in-context learning approaches that can achieve performance comparable to that of task-specific models, even under ideal conditions. The second limitation is the artificial nature of our masking approach. In real-world applications, masking is likely to occur at the word level and targets sensitive information. Our method, however, employed subword-level random masking. Despite this fundamental difference, we believe our test set includes samples with realistically plausible masking since sub-word masking cumulatively approximates word-level masking, and sensitive information can also be obscured by randomly chosen. Our statistical analysis, which shows main diseases are masked in proportion to the corruption rate, also supports our hypothesis. Moreover, this approach allows for the systematic masking with which we produced four different test sets. We believe the insights derived from our experiments can provide valuable guidance for future research.

Acknowledgments

This work was supported by Institute of Information & communications Technology Planning & Evaluation (IITP) grant funded by the Korea government (MSIT) (RS-2022-00143911, AI Excellence Global Innovative Leader Education Program). Yoon JH has received grant support from NIH K23GM138984.

References

- Josh Achiam, Steven Adler, Sandhini Agarwal, Lama Ahmad, Ilge Akkaya, Florencia Leoni Aleman, Diogo Almeida, Janko Altschmidt, Sam Altman, Shyamal Anadkat, et al. Gpt-4 technical report. *arXiv preprint arXiv:2303.08774*, 2023.
- Monica Agrawal, Stefan Hegselmann, Hunter Lang, Yoon Kim, and David Sontag. Large language models are few-shot clinical information extractors. *arXiv preprint arXiv:2205.12689*, 2022.
- Jean-Baptiste Alayrac, Jeff Donahue, Pauline Luc, Antoine Miech, Iain Barr, Yana Hasson, Karel Lenc, Arthur Mensch, Katherine Millican, Malcolm Reynolds, et al. Flamingo: a

- visual language model for few-shot learning. *Advances in neural information processing systems*, 35:23716–23736, 2022.
- Anas Awadalla, Irena Gao, Josh Gardner, Jack Hessel, Yusuf Hanafy, Wanrong Zhu, Kalyani Marathe, Yonatan Bitton, Samir Gadre, Shiori Sagawa, et al. Openflamingo: An open-source framework for training large autoregressive vision-language models. *arXiv preprint arXiv:2308.01390*, 2023.
- Kathleen Benitez and Bradley Malin. Evaluating re-identification risks with respect to the hipaa privacy rule. *Journal of the American Medical Informatics Association*, 17(2): 169–177, 2010.
- William Berrios, Gautam Mittal, Tristan Thrush, Douwe Kiela, and Amanpreet Singh. Towards language models that can see: Computer vision through the lens of natural language. *arXiv preprint arXiv:2306.16410*, 2023.
- Adrian P Brady. Error and discrepancy in radiology: inevitable or avoidable? *Insights into Imaging*, 8(1):171–182, 2017. doi: 10.1007/s13244-016-0534-1.
- Michal Byra, Muhammad Febrian Rachmadi, and Henrik Skibbe. Few-shot medical image classification with simple shape and texture text descriptors using vision-language models. *arXiv preprint arXiv:2308.04005*, 2023.
- Wei-Lin Chiang, Zhuohan Li, Zi Lin, Ying Sheng, Zhanghao Wu, Hao Zhang, Lianmin Zheng, Siyuan Zhuang, Yonghao Zhuang, Joseph E Gonzalez, et al. Vicuna: An open-source chatbot impressing gpt-4 with 90%* chatgpt quality. See <https://vicuna.lmsys.org> (accessed 14 April 2023), 2(3):6, 2023.
- Chak Fong Chong, Xu Yang, Tenglong Wang, Wei Ke, and Yapeng Wang. Category-wise fine-tuning for image multi-label classification with partial labels. In *International Conference on Neural Information Processing*, pages 332–345. Springer, 2023.
- Wenliang Dai, Junnan Li, Dongxu Li, Anthony Meng Huat Tiong, Junqi Zhao, Weisheng Wang, Boyang Li, Pascale N Fung, and Steven Hoi. Instructblip: Towards general-purpose vision-language models with instruction tuning. *Advances in Neural Information Processing Systems*, 36, 2024.
- Jean-Benoit Delbrouck, Pierre Chambon, Christian Bluethgen, Emily Tsai, Omar Almusa, and Curtis P Langlotz. Improving the factual correctness of radiology report generation with semantic rewards. *arXiv preprint arXiv:2210.12186*, 2022.
- Jacob Devlin, Ming-Wei Chang, Kenton Lee, and Kristina Toutanova. Bert: Pre-training of deep bidirectional transformers for language understanding. *arXiv preprint arXiv:1810.04805*, 2018.
- Danny Driess, Fei Xia, Mehdi SM Sajjadi, Corey Lynch, Aakanksha Chowdhery, Brian Ichter, Ayzaan Wahid, Jonathan Tompson, Quan Vuong, Tianhe Yu, et al. Palm-e: An embodied multimodal language model. *arXiv preprint arXiv:2303.03378*, 2023.

- James E Feng, Afshin A Anoushiravani, Paul J Tesoriero, et al. Transcription error rates in retrospective chart reviews. *Orthopedics*, 43(5):e404–e408, 2020.
- Yu Gu, Robert Tinn, Hao Cheng, Michael Lucas, Naoto Usuyama, Xiaodong Liu, Tristan Naumann, Jianfeng Gao, and Hoifung Poon. Domain-specific language model pretraining for biomedical natural language processing. *ACM Transactions on Computing for Healthcare (HEALTH)*, 3(1):1–23, 2021.
- Jiaxian Guo, Junnan Li, Dongxu Li, Anthony Meng Huat Tiong, Boyang Li, Dacheng Tao, and Steven CH Hoi. From images to textual prompts: Zero-shot vqa with frozen large language models. *arXiv preprint arXiv:2212.10846*, 2022.
- Neil Houlsby, Andrei Giurgiu, Stanislaw Jastrzebski, Bruna Morrone, Quentin De Laroussilhe, Andrea Gesmundo, Mona Attariyan, and Sylvain Gelly. Parameter-efficient transfer learning for nlp. In *International conference on machine learning*, pages 2790–2799. PMLR, 2019.
- Edward J Hu, Yelong Shen, Phillip Wallis, Zeyuan Allen-Zhu, Yuanzhi Li, Shean Wang, Lu Wang, and Weizhu Chen. Lora: Low-rank adaptation of large language models. *arXiv preprint arXiv:2106.09685*, 2021.
- Yushi Hu, Hang Hua, Zhengyuan Yang, Weijia Shi, Noah A Smith, and Jiebo Luo. Prompt-cap: Prompt-guided task-aware image captioning. *arXiv preprint arXiv:2211.09699*, 2022.
- Saahil Jain, Ashwin Agrawal, Adriel Saporta, Steven QH Truong, Du Nguyen Duong, Tan Bui, Pierre Chambon, Yuhao Zhang, Matthew P Lungren, Andrew Y Ng, et al. Rad-graph: Extracting clinical entities and relations from radiology reports. *arXiv preprint arXiv:2106.14463*, 2021.
- Alistair EW Johnson, Tom J Pollard, Seth J Berkowitz, Nathaniel R Greenbaum, Matthew P Lungren, Chih-ying Deng, Roger G Mark, and Steven Horng. Mimic-cxr, a de-identified publicly available database of chest radiographs with free-text reports. *Scientific data*, 6(1):317, 2019.
- Seungone Kim, Se June Joo, Doyoung Kim, Joel Jang, Seonghyeon Ye, Jamin Shin, and Minjoon Seo. The cot collection: Improving zero-shot and few-shot learning of language models via chain-of-thought fine-tuning. *arXiv preprint arXiv:2305.14045*, 2023.
- Hugo Laurençon, Lucile Saulnier, Léo Tronchon, Stas Bekman, Amanpreet Singh, Anton Lozhkov, Thomas Wang, Siddharth Karamcheti, Alexander Rush, Douwe Kiela, et al. Obelics: An open web-scale filtered dataset of interleaved image-text documents. *Advances in Neural Information Processing Systems*, 36, 2024.
- Patrick Lewis, Myle Ott, Jingfei Du, and Veselin Stoyanov. Pretrained language models for biomedical and clinical tasks: Understanding and extending the state-of-the-art. In Anna Rumshisky, Kirk Roberts, Steven Bethard, and Tristan Naumann, editors, *Proceedings of the 3rd Clinical Natural Language Processing Workshop*, pages 146–157, Online, November 2020. Association for Computational Linguistics. doi: 10.18653/v1/2020.clinicalnlp-1.17. URL <https://aclanthology.org/2020.clinicalnlp-1.17>.

- Bo Li, Yuanhan Zhang, Liangyu Chen, Jinghao Wang, Fanyi Pu, Jingkang Yang, Chunyuan Li, and Ziwei Liu. Mimic-it: Multi-modal in-context instruction tuning. *arXiv preprint arXiv:2306.05425*, 2023a.
- Chunyuan Li, Cliff Wong, Sheng Zhang, Naoto Usuyama, Haotian Liu, Jianwei Yang, Tristan Naumann, Hoifung Poon, and Jianfeng Gao. Llava-med: Training a large language-and-vision assistant for biomedicine in one day. *Advances in Neural Information Processing Systems*, 36, 2024.
- Junnan Li, Dongxu Li, Silvio Savarese, and Steven Hoi. Blip-2: Bootstrapping language-image pre-training with frozen image encoders and large language models. In *International conference on machine learning*, pages 19730–19742. PMLR, 2023b.
- Valentin Liévin, Christoffer Egeberg Hother, Andreas Geert Motzfeldt, and Ole Winther. Can large language models reason about medical questions? *Patterns*, 2023.
- Chin-Yew Lin. Rouge: A package for automatic evaluation of summaries. In *Text summarization branches out*, pages 74–81, 2004.
- Haotian Liu, Chunyuan Li, Qingyang Wu, and Yong Jae Lee. Visual instruction tuning. *Advances in neural information processing systems*, 36, 2024.
- Pengfei Liu, Weizhe Yuan, Jinlan Fu, Zhengbao Jiang, Hiroaki Hayashi, and Graham Neubig. Pre-train, prompt, and predict: A systematic survey of prompting methods in natural language processing. *ACM Computing Surveys*, 55(9):1–35, 2023.
- Sachit Menon and Carl Vondrick. Visual classification via description from large language models. *arXiv preprint arXiv:2210.07183*, 2022.
- Michael Moor, Qian Huang, Shirley Wu, Michihiro Yasunaga, Yash Dalmia, Jure Leskovec, Cyril Zakka, Eduardo Pontes Reis, and Pranav Rajpurkar. Med-flamingo: a multimodal medical few-shot learner. In *Machine Learning for Health (ML4H)*, pages 353–367. PMLR, 2023.
- Harsha Nori, Yin Tat Lee, Sheng Zhang, Dean Carignan, Richard Edgar, Nicolo Fusi, Nicholas King, Jonathan Larson, Yanzhi Li, Weishung Liu, et al. Can generalist foundation models outcompete special-purpose tuning? case study in medicine. *arXiv preprint arXiv:2311.16452*, 2023.
- PJ Robinson, D Wilson, A Coral, A Murphy, and P Verow. Variation between experienced observers in the interpretation of accident and emergency radiographs. *British Journal of Radiology*, 72(856):323–330, Apr 1999. doi: 10.1259/bjr.72.856.10474490.
- Akshay Smit, Saahil Jain, Pranav Rajpurkar, Anuj Pareek, Andrew Y Ng, and Matthew P Lungren. Chexbert: combining automatic labelers and expert annotations for accurate radiology report labeling using bert. *arXiv preprint arXiv:2004.09167*, 2020.
- Yuxuan Sun, Chenglu Zhu, Sunyi Zheng, Kai Zhang, Zhongyi Shui, Xiaoxuan Yu, Yizhi Zhao, Honglin Li, Yunlong Zhang, Ruoqia Zhao, et al. Pathasst: Redefining

- pathology through generative foundation ai assistant for pathology. *arXiv preprint arXiv:2305.15072*, 2023.
- Dídac Surís, Sachit Menon, and Carl Vondrick. Vipergpt: Visual inference via python execution for reasoning. In *Proceedings of the IEEE/CVF International Conference on Computer Vision*, pages 11888–11898, 2023.
- Hugo Touvron, Thibaut Lavril, Gautier Izacard, Xavier Martinet, Marie-Anne Lachaux, Timothée Lacroix, Baptiste Rozière, Naman Goyal, Eric Hambro, Faisal Azhar, et al. Llama: Open and efficient foundation language models. *arXiv preprint arXiv:2302.13971*, 2023.
- Tao Tu, Shekoofeh Azizi, Danny Driess, Mike Schaekermann, Mohamed Amin, Pi-Chuan Chang, Andrew Carroll, Charles Lau, Ryutaro Tanno, Ira Ktena, et al. Towards generalist biomedical ai. *NEJM AI*, 1(3):AIoa2300138, 2024.
- Dave Van Veen, Cara Van Uden, Maayane Attias, Anuj Pareek, Christian Bluethgen, Malgorzata Polacin, Wah Chiu, Jean-Benoit Delbrouck, Juan Manuel Zambrano Chaves, Curtis P Langlotz, et al. Radadapt: Radiology report summarization via lightweight domain adaptation of large language models. *arXiv preprint arXiv:2305.01146*, 2023a.
- Dave Van Veen, Cara Van Uden, Louis Blankemeier, Jean-Benoit Delbrouck, Asad Aali, Christian Bluethgen, Anuj Pareek, Malgorzata Polacin, Eduardo Pontes Reis, Anna Seehofnerova, et al. Clinical text summarization: Adapting large language models can outperform human experts. *Research Square*, 2023b.
- Jason Wei, Xuezhi Wang, Dale Schuurmans, Maarten Bosma, Fei Xia, Ed Chi, Quoc V Le, Denny Zhou, et al. Chain-of-thought prompting elicits reasoning in large language models. *Advances in neural information processing systems*, 35:24824–24837, 2022.
- Penny F Whiting, Clare Davenport, Catherine Jameson, Margaret Burke, Jonathan A C Sterne, Chris Hyde, and Yoav Ben-Shlomo. How well do health professionals interpret diagnostic information? a systematic review. *BMJ Open*, 5(7), 2015. ISSN 2044-6055. doi: 10.1136/bmjopen-2015-008155. URL <https://bmjopen.bmj.com/content/5/7/e008155>.
- C Wu, X Zhang, Y Zhang, Y Wang, and W Xie. Towards generalist foundation model for radiology by leveraging web-scale 2d&3d medical data. arxiv [preprint]. 2023 [accessed on october 2, 2023].
- Chaoyi Wu, Xiaoman Zhang, Ya Zhang, Yanfeng Wang, and Weidi Xie. Towards generalist foundation model for radiology. *arXiv preprint arXiv:2308.02463*, 2023.
- Yujia Xie, Luowei Zhou, Xiyang Dai, Lu Yuan, Nguyen Bach, Ce Liu, and Michael Zeng. Visual clues: Bridging vision and language foundations for image paragraph captioning. *Advances in Neural Information Processing Systems*, 35:17287–17300, 2022.
- Ruyi Xu, Yuan Yao, Zonghao Guo, Junbo Cui, Zanlin Ni, Chunjiang Ge, Tat-Seng Chua, Zhiyuan Liu, Maosong Sun, and Gao Huang. Llava-uhd: an lmm perceiving any aspect ratio and high-resolution images. *arXiv preprint arXiv:2403.11703*, 2024.

- An Yan, Yu Wang, Yiwu Zhong, Zexue He, Petros Karypis, Zihan Wang, Chengyu Dong, Amilcare Gentili, Chun-Nan Hsu, Jingbo Shang, et al. Robust and interpretable medical image classifiers via concept bottleneck models. *arXiv preprint arXiv:2310.03182*, 2023.
- Zhengyuan Yang, Zhe Gan, Jianfeng Wang, Xiaowei Hu, Yumao Lu, Zicheng Liu, and Lijuan Wang. An empirical study of gpt-3 for few-shot knowledge-based vqa. In *Proceedings of the AAAI Conference on Artificial Intelligence*, volume 36, pages 3081–3089, 2022.
- Kai Zhang, Jun Yu, Zhiling Yan, Yixin Liu, Eashan Adhikarla, Sunyang Fu, Xun Chen, Chen Chen, Yuyin Zhou, Xiang Li, et al. Biomedgpt: A unified and generalist biomedical generative pre-trained transformer for vision, language, and multimodal tasks. *arXiv preprint arXiv:2305.17100*, 2023a.
- Yuhao Zhang, Derek Merck, Emily Tsai, Christopher D. Manning, and Curtis Langlotz. Optimizing the factual correctness of a summary: A study of summarizing radiology reports. In Dan Jurafsky, Joyce Chai, Natalie Schluter, and Joel Tetreault, editors, *Proceedings of the 58th Annual Meeting of the Association for Computational Linguistics*, pages 5108–5120, Online, July 2020. Association for Computational Linguistics. doi: 10.18653/v1/2020.acl-main.458. URL <https://aclanthology.org/2020.acl-main.458>.
- Zhuosheng Zhang, Aston Zhang, Mu Li, Hai Zhao, George Karypis, and Alex Smola. Multi-modal chain-of-thought reasoning in language models. *arXiv preprint arXiv:2302.00923*, 2023b.

Appendix A. Example of Prompt

Our prompt is composed of the role assignment, task description, two retrieved examples, and the test sample. Here we provide one example of the prompt that we used for our framework.

You are an expert medical professional. Write a concise summary of the following chest X-ray report. The text description of the X-ray images and the full report, named "Finding" will be provided. Focus on the key findings and diagnoses noted primarily in the image description, while also incorporating relevant details from the full report. The summary, named "Impression", should be concise and presented in correct English sentences.

Image description: There is Atelectasis in the image in 24.20 probability.

There is Cardiomegaly in the image in 1.82 probability.

There is Consolidation in the image in 3.99 probability.

There is Edema in the image in 0.80 probability.

There is Enlarged Cardiomeastinum in the image in 8.94 probability.

There is Fracture in the image in 10.79 probability.

There is Lung Lesion in the image in 7.47 probability.

There is Lung Opacity in the image in 18.30 probability.

There is No Finding in the image in 31.68 probability.

There is Pleural Effusion in the image in 3.73 probability.

There is Pleural Other in the image in 1.05 probability.

There is Pneumonia in the image in 4.88 probability.

There is Pneumothorax in the image in 6.48 probability.

There is Support Devices in the image in 10.13 probability.

Finding: The heart size is normal. The hilar and mediastinal contours are unremarkable. The lungs are well expanded and clear. There is no evidence of a pneumothorax or pleural effusion. The visualized osseous structures are unremarkable.

Impression: No acute cardiopulmonary processes. Specifically, no evidence of an infiltrative process suggestive of pneumonia.

Image description: There is Atelectasis in the image in 2.38 probability.

There is Cardiomegaly in the image in 0.39 probability.

There is Consolidation in the image in 0.76 probability.

There is Edema in the image in 0.10 probability.

There is Enlarged Cardiomeastinum in the image in 3.32 probability.

There is Fracture in the image in 7.94 probability.

There is Lung Lesion in the image in 1.50 probability.

There is Lung Opacity in the image in 4.21 probability.

There is No Finding in the image in 78.47 probability.

There is Pleural Effusion in the image in 0.62 probability.

There is Pleural Other in the image in 0.93 probability.

There is Pneumonia in the image in 0.78 probability.

There is Pneumothorax in the image in 1.96 probability.

There is Support Devices in the image in 9.13 probability.

Finding: The heart size is normal. The hilar and mediastinal contours are unremarkable. The lungs are well expanded and clear. There is no evidence of a pneumothorax or pleural effusion. The visualized osseous structures are unremarkable.

Impression: Normal chest x-ray. Specifically, no pulmonary evidence of TB.

Image description: There is Atelectasis in the image in 4.65 probability.

There is Cardiomegaly in the image in 0.89 probability.

There is Consolidation in the image in 1.28 probability.
There is Edema in the image in 0.21 probability.
There is Enlarged Cardiomeastinum in the image in 4.43 probability.
There is Fracture in the image in 14.87 probability.
There is Lung Lesion in the image in 4.14 probability.
There is Lung Opacity in the image in 5.80 probability.
There is No Finding in the image in 45.93 probability.
There is Pleural Effusion in the image in 3.02 probability.
There is Pleural Other in the image in 3.44 probability.
There is Pneumonia in the image in 1.32 probability.
There is Pneumothorax in the image in 2.53 probability.
There is Support Devices in the image in 5.05 probability.
Finding: The heart size is normal. The hilar and mediastinal contours are unremarkable. The lungs are slightly hyperinflated, however appear to be clear. There is no evidence of pneumothorax or pleural effusions. The visualized osseous structures are unremarkable.
Impression: